Dalton Transactions

ROYAL SOCIETY OF CHEMISTRY

PAPER

View Article Online
View Journal | View Issue

Cite this: *Dalton Trans.*, 2022, **51**, 16596

Improved emission of Yb(III) ions in triazacyclononane-based macrocyclic ligands compared to cyclen-based ones†

Salauat R. Kiraev, [a] Emilie Mathieu, ‡[a] Daniel Kovacs,[a] Jordann A. L. Wells, [a] Monika Tomar,[a] Julien Andres *[b] and K. Eszter Borbas *[a]

Yb(III) complexes based on ligands with a 1,4,7-triazacyclononane (tacn) macrocyclic core were synthesised. The complexes carry a 4-methoxymethyl-substituted carbostyril chromophore that serves as a light-harvesting antenna. The ligands supply 5 nitrogen and 3 oxygen donors *via* 1 methylenecarboxamide and 2 picolinate donors, creating +1 charged complexes with an octadentate binding environment. The electronic properties of the picolinates are modulated by varying the substitution at the 4 position with OMe, H, Cl, or CF_3. Cyclic voltammetry indicated that the tacn-based Yb(III) complexes were easier to reduce than the analogous cyclen complexes. The first reductive event is likely picolinate-centred, followed by the formation of further reduced species. Antenna excitation yielded Yb(III) luminescence in the near-infrared (NIR) region in all cases. The antenna photophysical properties were consistent with intraligand photoinduced electron transfer from the excited carbostyril to the picolinate groups. The relative quantum yields of Yb(III) luminescence were determined. The lowest value was obtained for the complex with the most efficient antenna-to-picolinate photoinduced electron transfer. Despite intraligand electron transfer quenching of the antenna, the tacn-based Yb complexes were more emissive than their cyclen analogues, highlighting the influence of the ligand structure on the luminescence properties of NIR emissive lanthanide(III) ions.

Received 13th July 2022,
Accepted 28th September 2022

DOI: 10.1039/d2dt02266d

rsc.li/dalton

Introduction

Compounds emitting in the near infrared (NIR) are of great interest for a wide variety of applications from telecommunications[1] to thermometry[2] and bioimaging.[3,4] NIR emitting organic fluorophores and transition metal-based phosphors have several attractive properties. These include their tuneable excitation and emission wavelengths,[5–8] and that they can be rendered aqueous,[9] or fluorous soluble,[10,11] environment sensitive or analyte responsive,[4] and can incorporate reactive groups for labelling.[12] A common drawback, however, is their oxygen sensitivity, which results in decreased brightness, rapid fluorophore degradation, and the generation of cytotoxic reactive oxygen species.[13]

Several trivalent lanthanides (Ln) emit in the NIR.[14] Of these, Nd and Yb have emissions that are sufficiently robust for applications in aqueous media. Numerous Yb and Nd-based coordination compounds,[15–24] including some with inner-sphere solvent molecules,[25] have useful luminescence outputs in water. Ln(III) luminescence originates from 4f–4f transitions,[26,27] and direct Ln excitation is inefficient due to their low absorption coefficients. Ln(III) sensitisation is possible *via* a light-harvesting antenna.[26] In the case of Nd and Yb, visible-absorbing antennae can be used,[28–31] which is advantageous for minimising tissue damage in cellular applications. Even 2-photon excitation of antennae with only UV or blue absorption has been demonstrated using red light.[18,19,32,33] Ln(III) luminescence spectra consist of one or more sharp peaks with well-defined positions that are minimally influenced by the coordination environment. Ln excited states are long-lived. Eu and Tb emit with ms lifetimes, but even the shorter lifetimes (hundreds of ns) of Yb and Nd emission are longer than what is typical for cellular autofluorescence. Therefore, time-resolved detection of Ln signals is typically straightforward and is used in *e.g.* confocal microscopy.[34] Crucially, unlike

[a]*Department of Chemistry, Ångström Laboratory, Uppsala University, Box 523, 75120 Uppsala, Sweden. E-mail: eszter.borbas@kemi.uu.se*
[b]*Chemistry and Chemical Engineering Section, Ecole Polytechnique Fédérale de Lausanne (EPFL), BCH 3311, CH-1015 Lausanne, Switzerland. E-mail: julien.andres@epfl.ch*

†Electronic supplementary information (ESI) available. CCDC 2095001 and 2095002. For ESI and crystallographic data in CIF or other electronic format see DOI: https://doi.org/10.1039/d2dt02266d

‡Current address: Laboratoire de Chimie de Coordination du CNRS, UPR 8241, 31077 Toulouse, France.

organic-based fluorophores and transition metal-based phosphors, Ln emitters are usually not sensitive to oxygen quenching.[35] The brightness of Ln luminescence depends on the absorption coefficient of the antenna at the excitation wavelength, the Ln(III) sensitisation, and the efficiency of radiative decay of the Ln excited state compared to the other deactivation.[27] Modulation of these parameters enables the creation of analyte-sensitive probes.[16,33,36,37]

The Ln(III) sensitization mechanism depends on the Ln, the antenna, and their relative arrangement (Fig. 1). Resonance energy transfer is possible to Ln(III) receiving states that are not more than ~5000 cm^{-1} lower in energy than the antenna (S_1) or triplet (T_1) excited states. For Yb(III) with its excited state at ~10 000 cm^{-1}, this means an antenna with S_1 or T_1 ~15 000 cm^{-1}.[27] A second mechanism, originally proposed by Horrocks, begins with photoinduced electron transfer (PeT) from the excited antenna to Yb(III); back electron transfer (BeT) yields the ground state antenna and the excited state Yb(III).[38] A third mechanism was proposed by Crosby and Kasha in some cases when there is a large energy gap between a UV-absorbing antenna and the Yb(III) excited state:[39] the dissipation of the excess energy to the solvent or the lattice vibrational modes.[40] Such phonon-assisted energy transfer (PAEnT) could explain the observation of sensitised Yb emission in complexes wherein the first electron transfer of the Horrocks pathway is not thermodynamically favoured (Fig. 1).[41]

The efficiency of sensitised Ln(III) emission quantum yield (Φ_{Ln}) is dependent on the combined efficiencies of two consecutive stages. The first is the population of the Ln(III) excited state (Ln(III)*) *via* either the antenna's first singlet (S_1) or first triplet (T_1) excited states (η_{sens} in eqn (1)). The second stage is the emission of photons from the excited Ln ion. The latter is in competition with quenching pathways such as internal conversion, quenching by X–H oscillators (X = O, N, C), and, if the Ln(III)*–T_1 energy gap is small (<2000 cm^{-1}), thermal back energy transfer (BET).[42–44] The vibrational overtones of C–H, N–H and O–H do not influence the energy transfer from the ligand to emitting level of lanthanide. The efficiency of photon emission by excited Ln ions is defined by the intrinsic quantum yield (Φ_{Ln}^{Ln}), which is characteristic of the ion in a particular environment. All else being equal, shorter radiative lifetimes (τ_{rad}) yield higher Φ_{Ln}^{Ln}, and lead to higher Φ_{Ln}. The τ_{rad} of an Ln ion is determined by the refractive index of the medium and by the dipole moments of the transitions, which are affected by the coordination geometry. Lns have high coordination numbers (CN), and Ln–ligand interactions are mostly Coulombic. Therefore, the Ln coordination environment is governed by steric factors, and is a function of the ligand and of the solvent. The shortening of τ_{rad} has been previously demonstrated for Eu(III) emitters as a viable strategy for improving Ln luminescence.[45–47] The calculation of τ_{rad} for Eu(III) is possible from the corrected luminescence spectrum,[48] however, this straightforward method is not available for the other Lns.[27,49]

$$\Phi_{Ln} = \Phi_{Ln}^{Ln} \cdot \eta_{sens} \quad (1)$$

$$\Phi_{Ln}^{Ln} = \frac{\tau_{rad}}{\tau_{obs}} \quad (2)$$

Octadentate ligands based on two different macrocycles [cyclen (1,4,7,10-tetraazacyclododecane), and tacn (1,4,7-triazacyclononane)] and completed with methylenecarboxylate or picolinate donors and 1 inner-sphere water molecule yield Eu(III) emitters with τ_{rad} ~5.40 and ~2.90 ms, respectively.[46,47] The beneficial effect of the shorter τ_{rad} on Φ_{Ln} in the tacn complexes was masked by two quenching processes: PeT from the excited antenna (Ant*) to the reducible Eu(III), and intraligand electron transfer from Ant* to the picolinates.[46] For Yb(III), antenna-to-Ln(III) PeT and the subsequent back electron transfer (BeT) can yield Yb(III)*, so unlike in the case of most Eu complexes,[50] PeT can be sensitising (Fig. 1).[38]

In this study, we have prepared the Yb(III) complexes of 4 carbostyril-appended tacn-based octadentate ligands bearing 2 picolinate coordinating moieties (**YbL^X**, Fig. 2a). We characterised them by ^{1}H NMR spectroscopy and X-ray crystallography, measured their redox properties by cyclic voltammetry and evaluated their luminescence efficiencies relative to each other as well as to cyclen-based complexes carrying the same antenna (**YbLc**, Fig. 2b). We constructed model compounds (**Py^X** in Fig. 2a) that enabled the study of the redox properties of the picolinate units in isolation. Based on these data, the possible contributions of the Horrocks sensitisation route (*i.e.* the combined PeT and BeT processes in Fig. 1), of the quenching intraligand PeT, and sensitisation by phonon-assisted energy transfer (PAEnT)[39] were assessed.

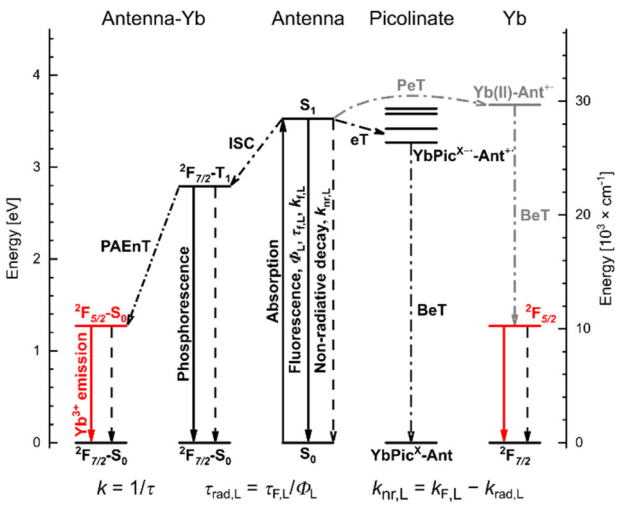

Fig. 1 Competing sensitising and quenching processes in photoexcited **YbL^X** complexes; solid and dashed lines indicate radiative and non-radiative processes, respectively.

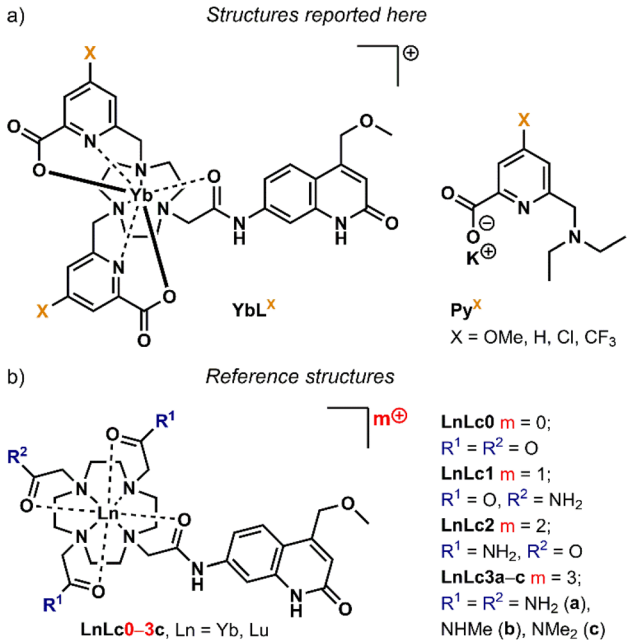

Fig. 2 (a) Complexes studied here (YbL^X) and pyridine model compounds (Py^X), X is the pyridine *p*-substituent. (b) Cyclen-based Yb complexes used as the reference structures (**YbLc**), **LnLc0–3c** are cyclen-based complexes with 0 to +3 overall charge.

Results and discussion

Solution and solid-state structures

Previously reported ligands $\mathbf{L^X}$ (X = OMe, H, Cl, CF_3)[46] were reacted with $YbCl_3$ in H_2O : EtOH 1 : 1 mixture for 16 h at 45 °C to yield $\mathbf{YbL^X}$. The products were purified by column chromatography on neutral alumina.[46,51] Potassium pyridine-2-carboxylate model compounds $\mathbf{Py^X}$ were synthesised from known 4-substituted methyl 6-(bromomethyl)picolinates in two steps in excellent yield (Schemes S1 and S2†). $\mathbf{Py^X}$ were fully characterised by ^{1}H, ^{13}C, and ^{19}F NMR spectroscopies and high-resolution mass spectrometry (HR-MS), while the complexes were characterised using HPLC-MS, HR-MS, paramagnetic ^{1}H NMR spectroscopy, and UV-Vis absorption and emission spectroscopies, as well as single crystal X-ray crystallography in the case of $\mathbf{YbL^H}$ and $\mathbf{YbL^{CF3}}$. Analytical data confirmed the formulae and general structures of $\mathbf{Py^X}$ and $\mathbf{YbL^X}$.

Paramagnetic ^{1}H NMR spectroscopy of Yb(III) coordination compounds can be very informative, and several tacn-based Yb(III) chelates have recently been analysed.[52] The ^{1}H NMR spectra of $\mathbf{YbL^X}$ consisted of 31–37 individual signals, which is consistent with the presence of both enantiomers (*vide infra*) of a single diastereomer for all four complexes, for which 34–36 individual signals are expected, or with several species rapidly interconverting on the NMR timescale (Fig. S5–S9†). Our attempts to fully assign the spectra were unsuccessful. Based on literature precedent, the broadened peaks >30 ppm are ascribed to protons on methylene spacers between tacn and picolinate groups, while the sharp signals at <−25 ppm are assigned to axial CH_2 protons of the 9-membered ring.[53] These signals are common to all four complexes. The pyridine *para*-substituents are far removed from the Yb(III), and their electronic effects are not expected to have a dramatic influence on picolinate coordination to the metal.[46] Parker has demonstrated the high sensitivity of the ^{1}H NMR shifts to solvation and the ligand field in tacn-based tris-picolinate Yb(III) complexes.[54] Thus, the ~10 ppm differences in the most and least deshielded signals in $\mathbf{YbL^H}$ and $\mathbf{YbL^{CF3}}$ are unsurprising and consistent with the metals occupying similar coordination geometries. The presence of at least two species in solution is also confirmed by two resonances in ^{19}F NMR spectrum of $\mathbf{YbL^{CF3}}$ both attributable to CF_3-groups from different complex isomers (Fig. S10†).

FT-IR spectra were recorded on solid samples (Fig. S11–S14†) and displayed a broad absorption band between 3600–2800 cm^{-1} corresponding to O–H stretching vibration bands, with some sharp features that can be attributed to N–H and C–H stretching vibration bands. Strong absorption bands due to stretches of C=O bonds, likely of the carboxylate groups, were also observed at 1637, 1610, 1654, 1651 cm^{-1} for $\mathbf{YbL^H}$, $\mathbf{YbL^{OMe}}$, $\mathbf{YbL^{Cl}}$, and $\mathbf{YbL^{CF3}}$, respectively.

Single crystals suitable for X-ray diffraction analysis were obtained by vapor diffusion of glyme and dioxane into concentrated aqueous solutions of $\mathbf{YbL^{CF3}}$–**F**, and $\mathbf{YbL^H}$, respectively. Crystals of $\mathbf{YbL^{CF3}}$–**F** were grown in the presence of 1 equiv. of potassium fluoride. Compounds $\mathbf{YbL^H}$ (Fig. 3) and $\mathbf{YbL^{CF3}}$–**F** (Fig. S15†) possess a central Yb atom with a nine-coordinate geometry in a (heavily) distorted tricapped trigonal prismatic arrangement, as seen in related complexes.[46] The trigonal prism is capped by two tethered carboxylate groups and a flu-

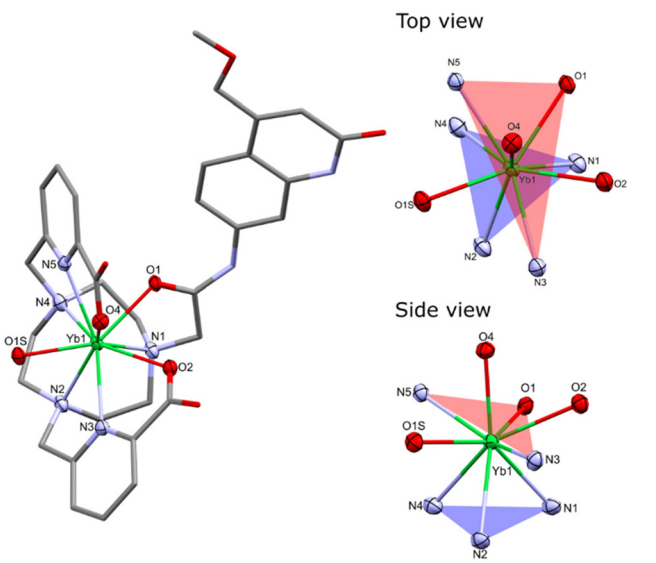

Fig. 3 Solid-state structure (left) and the coordination environment of Yb from the top and side view (right) in $\mathbf{YbL^H}$. H atoms, non-coordinating Cl^- counterions and water molecules were omitted for clarity. Ellipsoids displayed at 50% probability for atoms of the coordination environment, the rest of the molecule is depicted as capped sticks.

oride (for $\mathbf{YbL^{CF3}}$–F) or a water molecule (for $\mathbf{YbL^{H}}$). The two planes of the trigonal prism are comprised of the N-donors of the tacn ligand (N1, N2, N3 for $\mathbf{YbL^{CF3}}$–F/N4 $\mathbf{YbL^{H}}$; N_{3PL}), or of the antenna amide O- and the pyridine N-donors (N3 for $\mathbf{YbL^{H}}$/N4 for $\mathbf{YbL^{CF3}}$–F, N5, O1; NNO_{PL}). As previously observed, the two planes are not parallel with N_{3PL}–Ln–NNO_{PL} angles ranging 123–125°. These values are slightly wider than those of related Eu-, Gd- and Tb-complexes previously reported.[46] In addition, the Yb centre sits further from the NNO_{PL} (Ln–NNO_{PL} ~0.65 Å (Yb) *vs.* ~0.3 Å (Eu, Gd, Tb)) and closer to the N_{3PL} (Ln–N_{3PL} 1.967(2) to 1.9860(15) Å (Yb) *vs.* 2.017(4) to 2.065(4) Å (Eu, Gd, Tb)). These differences are likely to arise from the shorter ionic radius of Yb^{3+} (for CN = 9, 1.04 Å) than that of lighter Ln^{3+} ions (CN = 9, Eu^{3+} 1.12 Å, Gd^{3+} 1.11 Å, Tb^{3+} 1.10 Å).[55] Both $\mathbf{YbL^{CF3}}$–F and $\mathbf{YbL^{H}}$ are racemic in the solid state, containing $\Lambda(\delta\delta\delta)$ and $\Lambda(\lambda\lambda\lambda)$ isomers in the unit cell (Table S1†).[52]

The bond metrics are shorter than those reported for related Ln^{3+} carbostyril-substituted tacn and cyclen complexes,[46,51] which is consistent with the smaller ionic radius of Yb^{3+}. The Yb–O and Yb–N bond distances in $\mathbf{YbL^{CF3}}$–F are slightly elongated when compared to those in $\mathbf{YbL^{H}}$, which can be ascribed to the presence of the fluoride co-ligand shielding the Yb charge in the former, although electronic differences between the macrocyclic ligands may also play a role. The Yb–N_{tacn} distances range 2.513(3)–2.649(4) Å, while the Yb–N_{PY} distances range 2.456(2)–2.512(2) Å. The Yb–O distances of the carboxylates range 2.306(2)–2.389(2) Å, and the Yb–O(amide) distances vary 2.355(2)–2.400(2) Å. The Yb–F and Yb–OH_2 distances of 2.110(2) and 2.313(2)–2.326(2) Å, respectively, are shorter than those of related Ln^{3+} tacn- and cyclen-based complexes (averages: Ln^{3+}–F, 2.203(3) Å; Ln^{3+}–OH_2, 2.404(4) Å), but the differences are consistent with the smaller ionic radius of Yb^{3+} (Table S2†).[46,51]

The CN and geometry of the complexes depend on the structure of the ligand. The X-ray structures of $\mathbf{YbL^{CF3}}$–F and $\mathbf{YbL^{H}}$ show that these two species have CN = 9 and adopt a distorted tricapped trigonal prismatic arrangement, whereas the cyclen-based complexes were twisted square antiprismatic (TSAP) with CN = 8.[56] The ^{1}H NMR spectra of $\mathbf{YbL^{X}}$ are consistent with all the complexes adopting the same geometry in solution. For both sets of ligands, we can assume that changes in photophysical properties within a series will be due to changes in redox properties rather than structural differences.

Electrochemistry

The metal- and ligand-based redox properties of the complexes were studied by cyclic voltammetry. Experiments were carried out on the complete library of Yb(III) complexes, as well as with a series of model compounds with only a picolinate moiety (Fig. 2a). The latter were designed to enable the identification of Yb and pyridine-based redox events. Analyses were performed at 0.1 V s^{-1} scan rate in DMF containing 0.1 M $(n\text{-Bu})_4NClO_4$ as the electrolyte. DMF has a more suitable solvent window than water to study Yb(III) reduction. Voltammograms were recorded by scanning first towards more negative potential values (reduction). A glassy carbon electrode and a Ag/Ag^+ reference electrode (0.01 M $AgNO_3$ in MeCN) were used. Ferrocene was used as a pseudo-reference and was added at the end of the experiment. The peak anodic and cathodic potentials (E_{pa}, E_{pc}) values *vs.* F_c/F_c^+ and *vs.* NHE are reported in Table S4.†

The electrochemical properties of $\mathbf{YbL^{X}}$ were explored along with those of *p*-substituted picolinate models $\mathbf{Py^{X}}$ (Fig. S17 and S18†). Compounds $\mathbf{Py^{X}}$ display an irreversible reduction wave with E_{pc} values from −1.66 to −1.46 V *vs.* NHE that follow the order $\mathbf{Py^{OMe}}$ < $\mathbf{Py^{H}}$ < $\mathbf{Py^{Cl}}$ < $\mathbf{Py^{CF3}}$. This wave was attributed to the substituted pyridine reduction, which is easier for the picolinate with a stronger electron withdrawing group (Table 1).[57,58] An oxidation wave at ~0.94 V *vs.* NHE is common to all $\mathbf{Py^{X}}$, and may correspond to the oxidation of the tertiary 6-amino group (Table S4†).[59] $\mathbf{YbL^{X}}$ display several reductive events and no oxidation wave (Fig. S18†). The first reduction wave in these complexes range from −1.88 to −1.51 V *vs.* NHE and similarly follows the order $\mathbf{YbL^{OMe}}$ < $\mathbf{YbL^{H}}$ < $\mathbf{YbL^{Cl}}$ < $\mathbf{YbL^{CF3}}$. As a comparison, picolinate reduction in $\mathbf{GdL^{X}}$ in 100 mM aqueous NH_4Cl solution under Ar occurred between E_{red} = −1.43 V *vs.* NHE (for X = OMe) and −1.13 V *vs.* NHE (for X = CF_3),[46] and shows a similar trend in E_{pc} value of the first reduction wave (OMe < H < Cl < CF_3, Table 1). The acetylated 4-methoxymethyl carbostyril antenna has a reduction potential of −2.22 V *vs.* NHE measured in identical conditions as $\mathbf{YbL^{X}}$.[56] This entity is probably not involved in the reductive event observed in $\mathbf{YbL^{X}}$ complexes. The first reduction wave may be either due to the reduction of a picolinate moiety or of Yb(III).

A linear variation of E_{pc} *versus* Hammett substituent constants σ_p is observed for $\mathbf{YbL^{X}}$ and $\mathbf{Py^{X}}$, similarly to what has previously been observed for $\mathbf{GdL^{X}}$ (Fig. S19†).[46] This indicates that the *p*-substituents have a strong influence on the electron-accepting ability of $\mathbf{YbL^{X}}$, and the greater electron accepting ability of the picolinate moieties shifts E_{pc} to more positive values. The impact of the substituent is larger in $\mathbf{YbL^{X}}$ and $\mathbf{GdL^{X}}$ complexes compared to the model compounds and seems to depend on the Lewis acidity of the metal ion as $\Delta E_{pc}(CF_3$ *vs.* OMe) = 0.37 V for $\mathbf{YbL^{X}}$, 0.30 V for $\mathbf{GdL^{X}}$, and 0.20 V for $\mathbf{Py^{X}}$.

All tacn-based $\mathbf{YbL^{X}}$ cyclic voltammograms contain several irreversible reductive events that happen at close potentials

Table 1 Picolinate-based reduction potentials in $\mathbf{YbL^{X}}$, $\mathbf{Py^{X}}$ and $\mathbf{GdL^{X}}$

Complex	E_{red} [V *vs.* NHE][a]	Model compound	E_{red} [V *vs.* NHE][a]	Complex	E_{red} [V *vs.* NHE][b]
$\mathbf{YbL^{OMe}}$	−1.88	$\mathbf{Py^{OMe}}$	−1.66	$\mathbf{GdL^{OMe}}$	−1.43
$\mathbf{YbL^{H}}$	−1.82	$\mathbf{Py^{H}}$	−1.61	$\mathbf{GdL^{H}}$	−1.36
$\mathbf{YbL^{Cl}}$	−1.66	$\mathbf{Py^{Cl}}$	−1.52	$\mathbf{GdL^{Cl}}$	−1.21
$\mathbf{YbL^{CF3}}$	−1.51	$\mathbf{Py^{CF3}}$	−1.46	$\mathbf{GdL^{CF3}}$	−1.13

[a] Measured in DMF in glovebox with 0.1 M NBu_4ClO_4 as a supporting electrolyte and at 0.1 V s^{-1} scan rate. [b] Measured in H_2O with 0.1 M NH_4Cl as a supporting electrolyte under Ar at 0.1 V s^{-1} scan rate, from ref. 46.

(Fig. S18†), and could correspond to picolinate or Yb(III) reductions. The irreversibility of the first reduction wave in **YbL^{X}** suggest that the reduced **YbL$^{X}_{red}$** is not stable and that a chemical step takes place after the electron transfer. Due to this, it is impossible to determine the reduction potential of the Yb(III)/Yb(II) couple for **YbL^{X}**. Thus, the value of −1.92 V *vs.* NHE (E_{pc} for **YbLc1**) was used for the calculations of ΔG_{eT} for antenna to Yb(III) PeT, while E_{red} values of **YbL^{X}** (Table 1) were utilised to calculate intraligand PeT driving force in **YbL^{X}** complexes (*vide infra*).

Photophysical properties

The photophysical properties of the complexes were determined in aqueous 10 mM PIPES buffer at pH = 6.5 ([**LnL**] = 10 μM) to enable comparison with **LnLc**.[56] The results are summarised in Tables 2, 3, S5–S7, and Fig. 4, 5 and S20–S35.†

Ligand-centred photophysics. The luminescence spectra of all the Ln complexes were similar. The absorption spectra of **YbL^{X}** showed two bands at λ_{abs} = 274–279 nm and λ_{abs} = 330–331 nm, assigned to pyridine and carbostyril absorptions, respectively (Fig. S28†). The longer-wavelength absorption band was independent of the picolinate substitution pattern, indicating that the effects of the pyridine electronic properties on the carbostyril photophysics are negligible. The relative intensity, λ_{abs}, and the shape of the pyridine absorption band was strongly substituent-dependent. More electron poor **YbL^{CF3}** had larger intensity and red-shifted absorption of the picolinate band compared to that of **YbL^{H}**. In order to avoid variations due to the picolinate absorption of the complexes, **YbL^{X}** excitation was performed at 323–331 nm, where only the carbostyril chromophore absorbs.

Antenna excitation at λ_{ex} = 329 nm yielded antenna fluorescence with λ_{em} = 376 nm (Fig. S29†), along with Yb(III) luminescence in the NIR (*vide infra*). The shapes of the **YbL^{X}** carbostyril fluorescence spectra differed from those of cyclen-based complexes with the same antenna. Specifically, in the case of **YbL^{X}** an additional band is observed between 400–600 nm compared to **YbLc** (Fig. S22†). This band becomes stronger in the order **YbL^{H}** < **YbL^{OMe}** < **YbL^{Cl}** < **YbL^{CF3}**, and could indicate aggregation, or could be a twisted intramolecular charge transfer state of the carbostyril induced by steric, electrostatic, and/or photodynamic effects. A similar extra band has been observed in Ln complexes bearing multiple coumarin antennae in the coordination sphere,[60] and was shown to impact the photophysical properties of the Ln ions by facilitating either EnT or BET.

Table 2 Antenna fluorescence quantum yields of LnL complexes (Ln = Gd, Yb) and comparison to their cyclen-based +1-charged analogues

Complex	Φ_L [a,b] [%] (Rel. Φ_L [%])	Complex	Φ_L [a,c] [%] (Rel. Φ_L [%])	$\tau_{f,L}$ [ns] (**YbL^{X}**)
YbL^{OMe}	4.69 ± 0.18 (100)	**GdL^{OMe}**	6.85 (100)	0.26[d]
YbL^{H}	3.68 ± 0.04 (79)	**GdL^{H}**	6.42 (94)	0.20[e]
YbL^{Cl}	2.01 ± 0.02 (43)	**GdL^{Cl}**	4.64 (68)	<0.15[f]
YbL^{CF3}	0.99 ± 0.04 (21)	**GdL^{CF3}**	2.11 (31)	<0.15[f]
YbLc1	5.43 ± 0.05	**GdLc1**	7.01	0.34

[a] Determined relative to quinine sulfate (Φ = 0.59) in H_2SO_4 (0.05 M) in H_2O.[61] [b] Mean ± standard deviation for three independent measurements. [c] From ref. 51 (**GdLc1**) and ref. 46 (**GdL^{X}**). [d] χ^2 = 1.5600. [e] χ^2 = 1.5215. [f] Too short to measure.

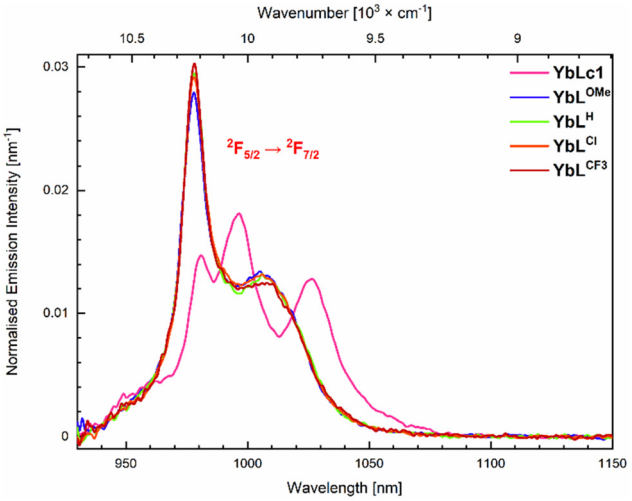

Fig. 4 Emission spectra of the Yb(III) complexes (A = 0.10) in 10 mM PIPES in H_2O, pH 6.5. λ_{ex} = 323 nm.

The antenna fluorescence residual quantum yields (Φ_L) were determined relative to quinine sulfate (Table 2). **YbL^{OMe}** with the most electron-rich OMe-substituted pyridines had the largest Φ_L, 4.69%, that of **YbL^{CF3}** was only 0.99%. These trends follow the ones seen in the Eu(III), Tb(III), and Gd(III) complexes of the same ligands.[46] The differences in Φ_L can be ascribed to PeT from the excited antenna to the pyridines, in addition to any PeT that may take place to Yb(III) (*vide infra*).[46] The larger Φ_L of **YbLc1** than that of **YbL^{X}** is consistent with intraligand PeT in the latter, which is also supported by the antenna fluorescence lifetimes ($\tau_{f,L}$). The $\tau_{f,L}$ are longer in **YbLc1** than in **YbL^{X}**, 0.34 ns and <0.26 ns, respectively (Tables 2, S7, Fig. S31 and S32†). For **YbL^{X}** with the most electron-deficient pyridines (X = Cl, CF_3) $\tau_{f,L}$ were too short to measure with the experimental setup available to us (the lowest measurable lifetime value was 0.15 ns).

The steady-state emission spectra at 77 K of **YbL^{X}** revealed structured fluorescence bands, and no phosphorescence was observed, unlike in the case of the Gd analogues (Fig. S33†). Hence, T_1 is completely quenched in **YbL^{X}** as it was also demonstrated for **YbLc** series. Notably, S_1/T_1 were ~0.36 for **GdL^{X}** which is indicative of similar intersystem crossing rates across the set of complexes with **L^{x}** ligands (Table S7†).

The photostabilities of **YbL^{X}** were determined by irradiation of their samples in the presence of atmospheric oxygen. The extent of complex degradation was estimated from the antenna fluorescence emission spectrum. Within the **YbL^{X}** series, **YbL^{OMe}** had the lowest emission intensity (78% from initial) after continuous light irradiation for 2 h (Fig. S34 and S35†). The other compounds retained 86–91% of their original emis-

sion intensity. These values are comparable to what has been observed for **EuL^{X}** for which both PeT and intraligand PeT are possible.[47] **YbL^{X}** are more photostable than **TbL^{X}**, the degradation of the latter likely proceeds through antenna T_1 repopulation *via* BET, which is not possible for **YbL^{X}**.[47]

Metal-based photophysics. Excitation of the antenna at 323 nm yielded Yb(III) emission between 930–1100 nm for every complex (Fig. 4). The shapes of the emission spectra were compared by normalising them relative to the integral intensity of the emission bands. The shape of the emission is different in these complexes from those based on cyclen ligands.[56] **YbL^{X}** have two observed transitions centred at 979 nm and 1006 nm rather than the three transitions observed for **YbLc0–3** indicating that the symmetry of the coordination sphere is not the same in the two series. This confirms the observations that in the solid state the cyclen-based structures adopt a TSAP geometry with a coordination number of 8, whereas **YbL^{CF3}–F** and **YbL^{H}** are in a distorted tricapped trigonal prismatic arrangement with a coordination number of 9.

The spectra of **YbL^{X}** are similar and only a small variation of the most energetic and intense transition is observed. Upon increasing the electron-withdrawing character of the picolinate *para*-substituent, the intensity of 979 nm transition increases, whereas that of 1006 nm is unchanged within the experimental error. The spectra of **YbL^{H}** and **YbL^{Cl}** are very close to each other.

The Yb(III) excitation spectra contain features ascribed to the antenna as well as the picolinates (Fig. 5). The high-energy component is picolinate-dependent, and the intensity of this excitation band increases from the **YbL^{OMe}** to **YbL^{Cl}**, **YbL^{H}** and **YbL^{CF3}**, which is 1.7-fold higher than the excitation of **YbL^{OMe}**. **YbL^{Cl}** and **YbL^{H}** have approximately the same excitation intensity but with **YbL^{H}** slightly higher and blue-shifted compared to **YbL^{Cl}**. The absorption spectra display a similar trend, so that the higher intensity may come only from the increased amount of absorbed light. If the picolinates are better sensitisers than the carbostyril antenna, the effect should be in the order of 10–30% according to the peak intensity difference observed between the absorption and the excitation.

The relative Ln(III) emission quantum yields (φ_{Ln}) were calculated compared to the strongest emitter **YbL^{Cl}** (Table 3). With one exception, **YbL^{X}** are overall more luminescent than **YbLc**, despite intraligand PeT quenching the antenna excited state, and an inner-sphere water molecule. **YbL^{OMe}** and **YbL^{H}** have similar quantum yields within experimental error, and **YbL^{Cl}** was found to have the largest quantum yield, albeit only 2–3 standard deviations higher than **YbL^{OMe}** and **YbL^{H}**. The electron-withdrawing picolinate *p*-CF_3 group is unfavourable to Yb(III) luminescence, and **YbL^{CF3}** has the lowest quantum yield, even lower than **YbLc1**. While electron-withdrawing groups in the ligand should induce a stabilisation of the more electron rich Yb(II), such effect appears to be overpowered by the negative consequences of the intraligand eT which is the most thermodynamically downhill process for **YbL^{CF3}** in the **YbL^{X}** series (Table S8†). The calculation of intraligand ΔG_{eT} was done with E_{red}(Pic/Pic$^{\bullet-}$) ranging from −1.88 V (**YbL^{OMe}**) to −1.51 V *vs.* NHE (**YbL^{CF3}**). The results were consistent with intraligand eT being least and most favourable in **YbL^{OMe}** (−0.04 eV) and **YbL^{CF3}** (−0.41 eV), respectively, which is consistent with the lowest φ_{Ln} and Φ_L for the latter complex.

This result suggests that having electron-withdrawing groups on the picolinates is indeed beneficial to the PeT

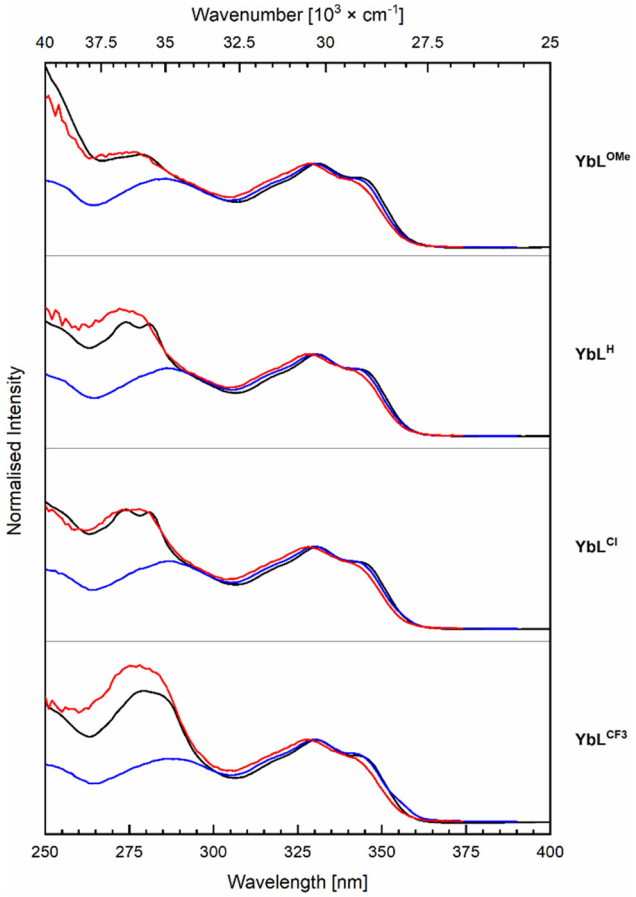

Fig. 5 Normalised excitation spectra for the Yb (red, λ_{em} = 978 nm) and antenna (blue, λ_{em} = 405 nm) emission with corresponding absorption (black) spectra of **YbL^{X}** complexes. Recorded in PIPES buffered (10 mM, pH 6.5, *A* = 0.10) aqueous solutions at r.t.

Table 3 Relative Yb(III) luminescence quantum yields of **YbL^{X}**

Complex	Relative φ_{Ln} [%] [a]
YbL^{OMe}	96 ± 2
YbL^{H}	94 ± 2
YbL^{Cl}	100
YbL^{CF3}	68 ± 1
YbLc1	81 (rel. to **YbLc3c**) 72 (rel. to **YbL^{Cl}**) [b]

[a] Measured in PIPES 10 mM, pH 6.5, upon excitation at 323 nm. [b] The luminescence intensity of **YbL^{X}** is related to the cyclen-based series by a factor 0.89(2), *i.e.* φ(**YbLc**)/φ(**YbL^{Cl}**) = 0.89(2) × φ(**YbLc**)/φ(**YbLc3c**).

antenna–Yb(III) pathway, but that the balance between the two PeT mechanisms, one quenching and one sensitising, is subtle. There is therefore probably not a lot of room for improvement of the PeT sensitised Yb(III) quantum yield by incorporating extra chromophores that are susceptible to photoredox processes.

Ln(III) are often assumed to have the antenna T_1 as the major feeding level,[26,62] although EnT from S_1 is also possible.[25,63–65] Neither T_1 (~22 500 cm^{-1})[25] nor S_1 (>27 500 cm^{-1}) in **YbL^{X}** appreciably overlap with the Yb(III) receiving level (10 260 cm^{-1}),[66] which excludes resonance EnT sensitisation. Therefore, PeT[38,41] or PAEnT[39] (Fig. 1) must be operating.

We have recently shown that in **YbLc1** and all its 0 to +3 charged analogues sensitisation can happen by PAEnT and by PeT. The contribution from PeT was probably small even in those +2 and +3 charged complexes where the initial PeT step of the mechanism was feasible. The thermodynamic feasibility of PeT as the first stage of this pathway was calculated (Table S9†). Due to the uncertainty of assigning E_{red}(Yb(III)/Yb(II)) in the cyclic voltammograms of **YbL^{X}**, calculations were performed with E_{red}(Yb(III)/Yb(II)) equal to −1.92 V *vs.* NHE. The latter value is E_{red}(Yb(III)/Yb(II)) for **YbLc1**. The reduction potential of Ln(III) are strongly dependent on the overall charge of the complex,[50,51,67] so the Yb(III) centre in **YbLc1** is a reasonable model for a +1 charged species. With E_{red}(Yb(III)/Yb(II)) of −1.92 V *vs.* NHE a ΔG(PeT) = 0 eV was obtained. The other, less negative E_{red} for Yb(III)/Yb(II) reduction values allowed for increasingly thermodynamically downhill processes.

The major sensitisation pathway of Yb(III) emission was still a question despite the suggested mechanisms (Fig. 1). Thus, we calculated the ratios of the Franck–Condon (FC) factors for the processes: ($^2F_{7/2}$–T_1) → ($^2F_{5/2}$–S_0), which ultimately leads to Yb(III) luminescence, and ($^2F_{7/2}$–T_1) → ($^2F_{7/2}$–S_0) that is responsible for the non-radiative deactivation of the complexes. The former was found to be 8 (**YbL^{H,Cl,CF3}**) to 9 (**YbL^{OMe}**) orders of magnitude faster than the latter (Tables S10 and S11†). Moreover, the ratio of FC factors for the same processes in **YbLc3c**, the strongest emitter of the **YbLc** series, was found to be identical to that of **YbL^{H,Cl,CF3}**. Hence, intraligand eT quenching in **YbL^{CF3}** (*vide supra*) offsets the improved φ_{Ln}, which was observed for the rest of the **YbL^{X}** series compared to the **YbLc**.

Another pathway to consider is the population of the $^2F_{5/2}$ receiving level *via* the Pic$^{\bullet-}$–Ant$^{\bullet+}$ state. This process would be feasible if eT yielding Yb(II)–Ant$^{\bullet+}$ from the initially formed Pic$^{\bullet-}$–Ant$^{\bullet+}$ is possible. The estimated energy difference E(Yb(II)–Ant$^{\bullet+}$) = E_{ox}^{Me} (**AcCS^{MOM}**)[46] − E_{red}^{Yb} (**YbLc1**) = 3.68 eV is larger than the potential difference for the intraligand eT, ranging from 3.64 eV (**YbL^{OMe}**) to 3.27 eV (**YbL^{CF3}**) (Table S8†). The difference is small for **YbL^{OMe,H,Cl}** (ΔE = 0.04–0.26 eV) and considerable for **YbL^{CF3}** (ΔE = 0.41 eV). Thus, the improved φ_{Ln} may come from the intermediate Pic$^{\bullet-}$–Ant$^{\bullet+}$ state formed after intraligand eT, which could contribute with additional sensitisation.

In short, $\Delta_r G$ for the direct Yb(III)–antenna PeT reaction is approximately 0, whereas for the intraligand PeT it is slightly to moderately negative and hence favourable. So intraligand PeT is more likely to happen, and is especially supposed to be prevalent for **YbL^{CF3}**, the least luminescent complex. While intraligand PeT thus does appear to be unfavourable for Yb(III) luminescence, **YbL^{Cl}** is the second most favoured for intraligand PeT and the most luminescent **YbL^{X}**. Without additional experiments the actual contribution of this process to the overall sensitisation mechanism in **YbL^{X}** is difficult to establish with certainty.

Conclusions

A series of Yb(III) coordination compounds based on a tacn macrocycle functionalised by a carbostyril antenna and two identical *para*-substituted picolinate derivatives was prepared. Solution and solid-state studies of the Yb(III) complexes revealed the presence of similar species with a nonadentate distorted tricapped trigonal prism coordination environment of the metal centre. The picolinate-based reductions in Yb(III) compounds took place from −1.88 to −1.51 V *vs.* NHE for the least and most electron-deficient ligands, respectively, which is in accordance with the expected substitution effect. Yb(III) emission was differently shaped compared to the one of the cyclen series, which is expected as the tacn- and cyclen-based complexes have different symmetries. The fluorescence of the antenna was altered by the different substituents on the picolinate, and the antenna Φ_L were consistent with PeT quenching of the carbostyril excited state by the electron-poor pyridines.

The quantum yields of the Yb(III) emission were higher than those of cyclen-based emitters. This was surprising as in **YbL^{X}** Yb(III) sensitisation was competing with antenna quenching by the picolinates. The higher Yb(III) luminescence could be the result of a an improvement in either of the two components contributing to the overall emission, namely (1) better sensitization, or (2) more efficient radiative decay of excited-state Yb(III), *i.e.* higher intrinsic quantum yield of **L^{X}**-bound Ln(III). The possibility of the latter is suggested by the comparison with the analogous Eu species for which Φ_{Ln}^{Ln} is readily determined: Φ_{Eu}^{Eu}(**EuL^{X}**) is larger than Φ_{Eu}^{Eu}(**EuLc**), ~17.5 and 11%, respectively.[7,51]

Yb(III) sensitisation was unlikely to proceed *via* resonance EnT due to the lack of spectral overlap between the antenna and the Yb(III) excited states. The initial antenna-to-Yb(III) PeT step of Horrock's PeT mechanism seemed to be thermodynamically neutral. Other PeT pathways may be sensitising, and could contribute to the increased Yb luminescence of **YbL^{X}**. According to our calculations the intraligand process is thermodynamically favourable, and should be upon recombination or further electron transfers sensitising for Yb. T_1 decay to Yb(III)*–S_0 *via* PAEnT appears to be a viable sensitisation pathway in these emitters. Future experiments to determine the Yb(III) radiative lifetimes and intrinsic quantum yields could determine the contribution made by the coordination environment to the overall improvement in luminescence. The measurement of Yb(III), and antenna S_1 and T_1 lifetimes and

rise times, and an analysis of triplet T–T absorption could show how the Yb(III) excited state is populated, and could directly show the contributions of the various sensitisation and quenching pathways.

Taken together, these results are relevant for emitter design in several ways. First, incorporating multiple antennae in the same complex is often employed to increase emitter brightness. Our results suggest that quenching by intraligand PeT should be considered, and if possible, avoided so as not to lose the benefit of the improved absorption. Second, the emission intensity from the Eu(III) and Tb(III) complexes of these tacn-based ligands were clearly inferior to the cyclen-based ones; the situation was reversed for Yb(III). This may be due to increased Φ_{Ln}^{Ln} resulting from a change in the complex coordination geometry, or an improvement in sensitisation, *e.g.* the fact that specifically for Yb, intraligand PeT could also be sensitising.

Conflicts of interest

There are no conflicts to declare.

Acknowledgements

This work was supported by the Swedish Research Council (project grant 2017-04077 to K. E. B.), Carl Tryggers Stiftelse för vetenskaplig forskning (post doc fellowship to E. M.), and the Knut och Alice Wallenbergs Stiftelse (Dnr: 2018.0066 and Dnr: KAW 2019.0071).

References

1 S. V. Eliseeva and J.-C. G. Bünzli, *Chem. Soc. Rev.*, 2009, **39**, 189–227.
2 A. V. Orlova, V. Y. Kozhevnikova, A. S. Goloveshkin, L. S. Lepnev and V. V. Utochnikova, *Dalton Trans.*, 2022, **51**, 5419–5425.
3 L.-L. Chen, L. Zhao, Z.-G. Wang, S.-L. Liu and D.-W. Pang, *Small*, 2022, **18**, 2104567.
4 M. Zhao, B. Li, H. Zhang and F. Zhang, *Chem. Sci.*, 2021, **12**, 3448–3459.
5 L. D. Lavis and R. T. Raines, *ACS Chem. Biol.*, 2008, **3**, 142–155.
6 L. D. Lavis and R. T. Raines, *ACS Chem. Biol.*, 2014, **9**, 855–866.
7 D. Ra, K. A. Gauger, K. Muthukumaran, T. Balasubramanian, V. Chandrashaker, M. Taniguchi, Z. Yu, D. C. Talley, M. Ehudin, M. Ptaszek and J. S. Lindsey, *J. Porphyrins Phthalocyanines*, 2015, **19**, 547–572.
8 K. M. Faries, J. R. Diers, J. W. Springer, E. Yang, M. Ptaszek, D. Lahaye, M. Krayer, M. Taniguchi, C. Kirmaier, J. S. Lindsey, D. F. Bocian and D. Holten, *J. Phys. Chem. B*, 2015, **119**, 7503–7515.
9 K. E. Borbas, V. Chandrashaker, C. Muthiah, H. L. Kee, D. Holten and J. S. Lindsey, *J. Org. Chem.*, 2008, **73**, 3145–3158.
10 E. M. Sletten and T. M. Swager, *J. Am. Chem. Soc.*, 2014, **136**, 13574–13577.
11 I. Lim, A. Vian, H. L. van de Wouw, R. A. Day, C. Gomez, Y. Liu, A. L. Rheingold, O. Campàs and E. M. Sletten, *J. Am. Chem. Soc.*, 2020, **142**, 16072–16081.
12 S. I. Reja, M. Minoshima, Y. Hori and K. Kikuchi, *Chem. Sci.*, 2021, **12**, 3437–3447.
13 A. P. Demchenko, *Methods Appl. Fluoresc.*, 2020, **8**, 022001.
14 Y. Ning, M. Zhu and J.-L. Zhang, *Coord. Chem. Rev.*, 2019, **399**, 213028.
15 E. R. Trivedi, S. V. Eliseeva, J. Jankolovits, M. M. Olmstead, S. Petoud and V. L. Pecoraro, *J. Am. Chem. Soc.*, 2014, **136**, 1526–1534.
16 S. Shuvaev and D. Parker, *Dalton Trans.*, 2019, **48**, 4471–4473.
17 A. Beeby, S. Faulkner, D. Parker and J. A. G. Williams, *J. Chem. Soc., Perkin Trans. 2*, 2001, 1268–1273.
18 A. T. Bui, M. Beyler, A. Grichine, A. Duperray, J.-C. Mulatier, Y. Guyot, C. Andraud, R. Tripier, S. Brasselet and O. Maury, *Chem. Commun.*, 2017, **53**, 6005–6008.
19 A. D'Aleo, A. Bourdolle, S. Brustlein, T. Fauquier, A. Grichine, A. Duperray, P. L. Baldeck, C. Andraud, S. Brasselet and O. Maury, *Angew. Chem., Int. Ed.*, 2012, **51**, 6622–6625.
20 A. D'Aleo, F. Pointillart, L. Ouahab, C. Andraud and O. Maury, *Coord. Chem. Rev.*, 2012, **256**, 1604–1620.
21 A. D'Aléo, A. Bourdolle, S. Brustlein, T. Fauquier, A. Grichine, A. Duperray, P. L. Baldeck, C. Andraud, S. Brasselet and O. Maury, *Angew. Chem., Int. Ed.*, 2012, **51**, 6622–6625.
22 M. F. K. Trautnitz, C. Doffek and M. Seitz, *ChemPhysChem*, 2019, **20**, 2179–2186.
23 C. Kruck, P. Nazari, C. Dee, B. S. Richards, A. Turshatov and M. Seitz, *Inorg. Chem.*, 2019, **58**, 6959–6965.
24 C. Doffek and M. Seitz, *Angew. Chem., Int. Ed.*, 2015, **54**, 9719–9721.
25 D. Kovacs, X. Lu, L. S. Mészáros, M. Ott, J. Andres and K. E. Borbas, *J. Am. Chem. Soc.*, 2017, **139**, 5756–5767.
26 A. de Bettencourt-Dias, in *Luminescence of Lanthanide Ions in Coordination Compounds and Nanomaterials*, John Wiley & Sons Ltd, 2014, pp. 1–48.
27 J.-C. G. Bünzli and S. V. Eliseeva, in *Lanthanide Luminescence: Photophysical, Analytical and Biological Aspects*, ed. P. Hänninen and H. Härmä, Springer Berlin Heidelberg, Berlin, Heidelberg, 2011, pp. 1–45.
28 N. M. Shavaleev, L. P. Moorcraft, S. J. A. Pope, Z. R. Bell, S. Faulkner and M. D. Ward, *Chem. Commun.*, 2003, 1134–1135.
29 S. J. A. Pope and R. H. Laye, *Dalton Trans.*, 2006, 3108–3113.
30 J.-Y. Hu, Y. Ning, Y.-S. Meng, J. Zhang, Z.-Y. Wu, S. Gao and J.-L. Zhang, *Chem. Sci.*, 2017, **8**, 2702–2709.
31 R. Xiong, D. Mara, J. Liu, R. Van Deun and K. E. Borbas, *J. Am. Chem. Soc.*, 2018, **140**, 10975–10979.

32 N. Hamon, A. Roux, M. Beyler, J.-C. Mulatier, C. Andraud, C. Nguyen, M. Maynadier, N. Bettache, A. Duperray, A. Grichine, S. Brasselet, M. Gary-Bobo, O. Maury and R. Tripier, *J. Am. Chem. Soc.*, 2020, **142**, 10184–10197.
33 J. H. S. K. Monteiro, N. R. Fetto, M. J. Tucker and A. de Bettencourt-Dias, *Inorg. Chem.*, 2020, **59**, 3193–3199.
34 S. Pandya, J. Yu and D. Parker, *Dalton Trans.*, 2006, 2757–2766.
35 A. Beeby, D. Parker and J. A. G. Williams, *J. Chem. Soc., Perkin Trans. 2*, 1996, 1565–1580.
36 L. Norel, O. Galangau, H. Al Sabea and S. Rigaut, *ChemPhotoChem*, 2021, **5**, 393–405.
37 Y. Ning, Y.-W. Liu, Y.-S. Meng and J.-L. Zhang, *Inorg. Chem.*, 2018, **57**, 1332–1341.
38 W. D. Horrocks Jr., J. P. Bolender, W. D. Smith and R. M. Supkowski, *J. Am. Chem. Soc.*, 1997, **119**, 5972–5973.
39 C. Reinhard and H. U. Güdel, *Inorg. Chem.*, 2002, **41**, 1048–1055.
40 G. A. Crosby and M. Kasha, *Spectrochim. Acta*, 1958, **10**, 377–382.
41 A. Beeby, S. Faulkner and J. A. G. Williams, *J. Chem. Soc., Dalton Trans.*, 2002, 1918–1922.
42 D. Mara, F. Artizzu, P. F. Smet, A. M. Kaczmarek, K. Van Hecke and R. Van Deun, *Chem. – Eur. J.*, 2019, **25**, 15944–15956.
43 I. Hernández and W. P. Gillin, in *Handbook on the Physics and Chemistry of Rare Earths*, ed. J.-C. Bünzli and V. K. Pecharsky, Elsevier, 2015, vol. 47, pp. 1–100.
44 E. Kreidt, C. Kruck and M. Seitz, in *Handbook on the Physics and Chemistry of Rare Earths*, ed. J.-C. G. Bünzli and V. K. Pecharsky, Elsevier, 2018, vol. 53, pp. 35–79.
45 S. V. Eliseeva, D. N. Pleshkov, K. A. Lyssenko, L. S. Lepnev, J.-C. G. Bunzli and N. P. Kuzmina, *Inorg. Chem.*, 2011, **50**, 5137–5144.
46 D. Kovacs, D. Kocsi, J. A. L. Wells, S. R. Kiraev and K. E. Borbas, *Dalton Trans.*, 2021, **50**, 4244–4254.
47 D. Kocsi, D. Kovacs, J. A. L. Wells and K. E. Borbas, *Dalton Trans.*, 2021, **50**, 16670–16677.
48 M. H. V. Werts, R. T. F. Jukes and J. W. Verhoeven, *Phys. Chem. Chem. Phys.*, 2002, **4**, 1542–1548.
49 A. Aebischer, F. Gumy and J.-C. G. Bünzli, *Phys. Chem. Chem. Phys.*, 2009, **11**, 1346–1353.
50 D. Kovacs and K. E. Borbas, *Coord. Chem. Rev.*, 2018, **364**, 1–9.
51 D. Kovacs, E. Mathieu, S. R. Kiraev, J. A. L. Wells, E. Demeyere, A. Sipos and K. E. Borbas, *J. Am. Chem. Soc.*, 2020, **142**, 13190–13200.
52 J. W. Walton, R. Carr, N. H. Evans, A. M. Funk, A. M. Kenwright, D. Parker, D. S. Yufit, M. Botta, S. De Pinto and K.-L. Wong, *Inorg. Chem.*, 2012, **51**, 8042–8056.
53 E. R. Neil, A. M. Funk, D. S. Yufit and D. Parker, *Dalton Trans.*, 2014, **43**, 5490–5504.
54 K. Mason, A. C. Harnden, C. W. Patrick, A. W. J. Poh, A. S. Batsanov, E. A. Suturina, M. Vonci, E. J. L. McInnes, N. F. Chilton and D. Parker, *Chem. Commun.*, 2018, **54**, 8486–8489.
55 R. D. Shannon, *Acta Crystallogr., Sect. A: Cryst. Phys., Diffr., Theor. Gen. Crystallogr.*, 1976, **32**, 751–767.
56 E. Mathieu, S. R. Kiraev, D. Kovacs, J. A. L. Wells, M. Tomar, J. Andres and K. E. Borbas, submitted.
57 M. D. C. Teixeira, F. S. Felix, S. S. Thomasi, Z. M. Magriotis, J. M. da Silva, L. L. Okumura and A. A. Saczk, *Microchem. J.*, 2019, **148**, 66–72.
58 J. A. Therrien and M. O. Wolf, *Inorg. Chem.*, 2017, **56**, 1161–1172.
59 J. Andrez, G. Bozoklu, G. Nocton, J. Pécaut, R. Scopelliti, L. Dubois and M. Mazzanti, *Chem. – Eur. J.*, 2015, **21**, 15188–15200.
60 J. Andres and K. E. Borbas, *Inorg. Chem.*, 2015, **54**, 8174–8176.
61 K. Suzuki, A. Kobayashi, S. Kaneko, K. Takehira, T. Yoshihara, H. Ishida, Y. Shiina, S. Oishi and S. Tobita, *Phys. Chem. Chem. Phys.*, 2009, **11**, 9850–9860.
62 M. Latva, H. Takalo, V.-M. Mukkala, C. Matachescu, J. C. Rodriguez-Ubis and J. Kankare, *J. Lumin.*, 1997, **75**, 149–169.
63 J. Andres and A.-S. Chauvin, *Phys. Chem. Chem. Phys.*, 2013, **15**, 15981–15994.
64 G. A. Hebbink, S. I. Klink, L. Grave, P. G. B. Oude Alink and F. C. J. M. Van Veggel, *ChemPhysChem*, 2002, **3**, 1014–1018.
65 C. Yang, L.-M. Fu, Y. Wang, J.-P. Zhang, W.-T. Wong, X.-C. Ai, Y.-F. Qiao, B.-S. Zou and L.-L. Gui, *Angew. Chem., Int. Ed.*, 2004, **43**, 5010–5013.
66 W. T. Carnall, G. L. Goodman, K. Rajnak and R. S. Rana, *J. Chem. Phys.*, 1989, **90**, 3443–3457.
67 S. R. Kiraev, E. Mathieu, F. Siemens, D. Kovacs, E. Demeyere and K. E. Borbas, *Molecules*, 2020, **25**, 5282.